

Thermoelectric Penta-Silicene with a High Room-Temperature Figure of Merit

Zhibin Gao* and Jian-Sheng Wang

Department of Physics, National University of Singapore, Singapore 117551, Republic of Singapore

E-mail: zhibin.gao@nus.edu.sg

Abstract

Silicon is one of the most frequently used chemical elements of the periodic table in nanotechnology.¹ Two-dimensional (2D) silicene, a silicon analog of graphene, has been readily obtained to make field-effect transistors since 2015.^{2,3} Recently, as new members of the silicene family, penta-silicene and its nanoribbon have been experimentally grown on Ag(110) surface with exotic electronic properties.⁴⁻⁶ However, the thermoelectric performance of penta-silicene has not been so far studied that would hinder its potential applications of electric generation from waste heat and solid-state Peltier coolers. Based on Boltzmann transport theory and *ab initio* calculations, we find that penta-silicene shows a remarkable room temperature figure of merit ZT of 3.4 and 3.0 at the reachable hole and electron concentrations, respectively. We attribute this high ZT to the superior “pudding-mold” electronic band structure and ultralow lattice thermal conductivity. The discovery provides new insight into the transport property of pentagonal nanostructures and highlights the potential applications of thermoelectric materials at room temperature.

Keywords

Ab initio calculations, penta-silicene, “pudding-mold” electronic structure, the figure of merit ZT , thermoelectric property

Introduction

The thermoelectric effect directly converts waste heat to electrical energy. Its efficiency is defined by a dimensionless figure of merit ZT , written as $ZT = S^2\sigma T/(\kappa_e + \kappa_L)$ in which S , σ , κ_e , κ_L are the Seebeck coefficient, electrical conductivity, electronic thermal conductivity and lattice thermal conductivity, respectively. Since S , σ , and κ_e are closely entangled with each other, it is challenging to increase numerator and decrease denominator concurrently, gaining a high ZT . Explicitly, an average ZT larger than 2 would make thermoelectric materials without toxic substances attractive and competitive when compared with other types of energy conversion.⁷ Furthermore, taking into account the application in daily life, near room temperature thermoelectric materials with high ZT are desirably needed.

A reduced κ_L can improve the thermoelectric efficiency, ZT .⁸ One can use resonant bonding,⁹ and lone electron pairs¹⁰ to reduce κ_L . Besides, the power factor $S^2\sigma$ can be augmented by electronic band engineering¹¹⁻¹³ and quantum confinement effect.¹⁴ Furthermore, 2D materials have inherent advantages to moderate the contradiction between S and σ due to the tunable electronic band gap, resulting in a high power factor. This is much simpler than in the case of bulk materials. In the case of 2D materials, one has great potential to break the

complicated relationship between S and σ due to the quantum confinement effect. This argument was firstly given by pioneer Mildred Dresselhaus.¹⁴ She also pointed out that one of the advantages of 2D layered materials is that one can actually engineer the band gap. In 2D, one can simply change the number of layers or apply stress/strain to modify the band gap, or even tune the chemical bond to modify the electronic band gap.¹⁴

In 2014, a theoretical work predicted a new 2D carbon allotrope called penta-graphene with favorable stability¹⁵ whose prototype was firstly proposed in iron-based material with exotic magnetic frustration.¹⁶ Afterward, the pentagonal system has attracted much attention, such as unexpected thermal conductivity,¹⁷⁻¹⁹ and seamless electrical contacts.²⁰ Recently, a stable penta-silicene was found by reducing the Coulomb interaction of silicon dimers.²¹ They also reported that it has ultrahigh Curie temperature of 1190 K. However, the thermoelectric performance of penta-silicene is still lacking.

In this study, we explore the thermoelectric property of penta-silicene based on the Boltzmann transport theory and *ab initio* calculations. It has good thermal, dynamical, and mechanical stability compared with many typical 2D materials. We find that penta-silicene has a nearly direct band gap of 0.68 eV at the DFT-HSE06 level. Lattice thermal conductivities of penta-silicene have values of 1.66 W/mK and 1.29 W/mK along x- and y-axis, respectively. At room temperature, Penta-silicene shows a maximum figure of merit ZT of 3.4 and 3.0 at the reachable hole and electron concentrations. Our work indicates that penta-silicene is a promising thermoelectric material, especially near room temperature.

Computational methods

We perform DFT calculations using projector-augmented-wave (PAW) method,^{22,23} Perdew-Burke-Ernzerhof (PBE)²⁴ and hybrid exchange-correlation HSE06 functional^{25,26} with default mixing parameter value $\alpha = 0.25$ in the VASP

code.²⁷⁻²⁹ Plane waves with 550 eV kinetic cutoff energy are used. The vacuum distance between the neighboring layer is set to be 20 Å removing the nonphysical long-range electrostatic interaction. The ionic Hellmann-Feynman forces in each atom and totally free energy are converged to 10^{-4} eV/Å and 10^{-8} eV in the structure optimization and band calculation. The Brillouin zone is sampled by uniform $21 \times 21 \times 1$. The electronic transport properties are calculated using the electronic Boltzmann transport theory implemented in BoltzTraP.³⁰ In the phonon calculation, we used $5 \times 5 \times 1$ supercell and $2 \times 2 \times 1$ k-point sampling to compute the second and third-order force constants. To solve the phonon Boltzmann transport equation, we adopted a $101 \times 101 \times 1$ Γ -centered q-grid. We also have tested the convergence of lattice thermal conductivity with respect to the cutoff radius, shown in the Supporting Information. The linearized phonon Boltzmann transport equation is solved by ShengBTE³¹ via a full iteration.

Results

Crystal structure

The optimized monolayer penta-silicene is shown in Figure 1a,b. There are 6 atoms in the primitive cell indicated by blue shading. From the top view, penta-silicene is the same as penta-graphene.¹⁵ But there is a little distortion of penta-silicene compared with penta-graphene.²¹ This is due to the tilting of silicon dimers in the penta-silicene in order to reduce the strong Coulomb repulsion and stabilize the crystal structure. It means that one cannot obtain the penta-silicene by simple element substitution. One should break the symmetry by moving one of the atoms in order to further lower the energy and reach a local minimum potential profile. The symmetry becomes $P2_1$ (space group no. 4) from $P42_1m$ (space group no. 113). The optimized lattice constants of penta-silicene and penta-graphene, shown in Table 1, are $|\vec{a}_1| = |\vec{a}_2| = 5.58$ Å and 3.64 Å, respectively, which are in good agreement with

Table 1: The calculated physical properties of penta-graphene and penta-silicene. $|\vec{a}_1|(|\vec{a}_2|)$ is the lattice constant. d and h are the intrinsic buckling distance and effective thickness. E_c is the cohesive energy per atom. C_{ij} is the elastic modulus tensor. G and ν are the shear modulus and Poisson’s ratio.

Materials	$ \vec{a}_1 (\vec{a}_2)$	d	h	E_c	C_{11}	C_{12}	G	ν
Unit	Å	Å	Å	(eV/atom)	(GPa)	(GPa)	(GPa)	—
penta-Gr	3.64	1.21	4.61	7.08	584.34	-46.88	328.94	-0.09
penta-Si	5.58	2.44	6.64	3.92	43.13	-23.56	30.31	-0.55

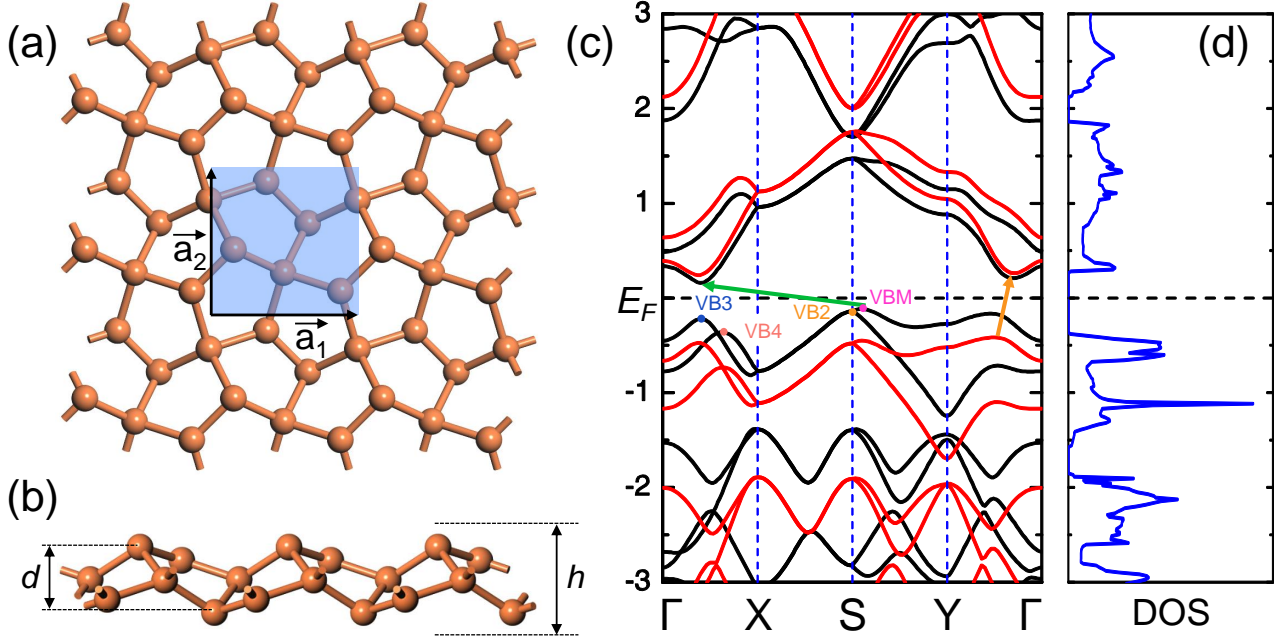


Figure 1: (a,b) Top and side views of the atomic structure of the monolayer penta-silicene in a 3×3 supercell. (c) Electronic band structure of penta-silicene using the DFT-PBE (black) and DFT-HSE06 (red) functionals. (d) Electronic density of states (DOS) at the HSE06 level. The indirect fundamental band gaps are marked by the green (PBE) and orange (HSE06) arrows in (c). The Fermi levels are set to zero. The sum of the intrinsic thickness d and two van der Waals radii of the outermost atom is defined as the effective thickness h . The primitive cell is indicated by blue shading in (a). Four hole pockets in valence bands around the Fermi level are labeled by different colors and numbers (VBM, VB2, VB3, and VB4). VBM denotes the valence band maximum. In the first Brillouin zone, the high symmetry k points are: $\Gamma(0\ 0\ 0)$, $X(1/2\ 0\ 0)$, $S(1/2\ 1/2\ 0)$ and $Y(0\ 1/2\ 0)$, respectively.

previous results.^{15,21} It is reasonable due to the augment of atomic size in the same main group IV. Intrinsically buckling distance also increases from 1.21 Å to 2.44 Å from penta-graphene to penta-silicene. The cohesive energy can be calculated by $E_c = (n * E_{Si} - E_0)/n$ in which E_{Si} , E_0 , and n are the energy of single silicon atom, the energy of the whole system at equi-

librium state, and the number of atoms in the system. The calculated E_c of penta-graphene and penta-silicene are 7.08 eV/atom and 3.92 eV/atom. Note that, in the experiment, E_c of the experimentally accessible silicene (hexagonal symmetry with 2 atoms in the primitive cell) and phosphorene are 3.71 eV/atom^{32,33} and 3.61 eV/atom,^{34,35} respectively. This in-

icates that the stability of penta-silicene is comparable with hexagonal silicene and black phosphorene, suggesting a robust chemical environment bond to maintain the stability of penta-silicene.

In 3D materials, the elastic tensor is a 6×6 tensor with 36 number of tensor elements. By considering the symmetry of the crystal structure, 6×6 tensor can be further simplified according to the specific crystal systems. There are 7 crystal systems in solid. The higher the symmetry of the crystal system, the smaller the number of independent tensor elements. For 2D materials, The elastic tensor is a 3×3 tensor. To be specific, the mechanical property has a close relationship with phonon modes on the crystal momentum near the center of the Brillouin zone.³⁶ For penta-silicene, there are 3 independent elastic components which are C_{11} , C_{12} and C_{66} . Note that the value of C_{66} is equal to the shear modulus G . The calculated mechanical data of penta-silicene is shown in Table 1. The elastic constants of any stable 2D materials must satisfy $C_{11}C_{22} - C_{12}^2 > 0$ and $C_{66} > 0$. From the table, it can be found that penta-silicene is mechanically stable. Furthermore, the value of C_{12} is -46.88 GPa, indicating a negative in-plane Poisson's ratio that is defined as³⁷ $\nu_{xy} = \frac{C_{21}}{C_{22}}$ and $\nu_{yx} = \frac{C_{12}}{C_{11}}$. For penta-graphene and penta-silicene, $C_{11} = C_{22}$ and $C_{12} = C_{21}$. C_{11} of penta-silicene is smaller than that of Si-*Cmma* of and Si-*Pmma*,³⁸ indicating a more flexible mechanical properties than other silicon allotropes. The calculated ν of penta-graphene and penta-silicene are -0.09 and -0.55 . The value of ν in penta-silicene is 5 times larger than that of penta-graphene. This mechanical property of negative Poisson's ratio is highly desirable for shock absorption in transistors.^{37,39}

Electronic band structure

The electronic band structure of penta-silicene is shown in Figure 1c,d. At PBE level (black), the indirect band gap indicated by the green arrow is 0.28 eV. Since the fundamental band gap is usually underestimated in DFT-PBE calculations, we also calculate it using HSE06 func-

tional (red). Overall, The entire energy bands are almost unchanged except for the shift up of the conduction bands and the shift down of the valence bands. Interestingly, the HSE06 band shows a nearly direct band gap of 0.68 eV indicated by the orange arrow. This change from the indirect-to-direct band gap would significantly enhance the optical absorbance.⁴⁰ Some top valence bands of monolayer penta-silicene around the Fermi level not only are quite close, but also are degenerate energetically. The conduction bands around the Fermi level have no similar behavior. We marked the "mountain peaks" of valence bands by different colors and numbers (VBM, VB2, VB3, and VB4). As a matter of fact, these degenerate valence bands will significantly enhance DOS and further Seebeck coefficient^{41,42} that directly enters the final figure of merit ZT . Furthermore, since the valence bands are highly degenerate, while conduction bands are non-degenerate, this leads to an asymmetric DOS in Figure 1d. This physical picture is known as "pudding-mold" and desirably required to achieve a large ZT .¹¹ We will further discuss it in the following.

Electronic transport properties

In order to obtain the electronic transport properties, such as Seebeck coefficient S , electrical conductivity σ , and electronic thermal conductivity κ_e , one has to compute the following quantities based on the Boltzmann transport theory, written as a function of the tensor \mathbf{K}_n ^{30,42}

$$\mathbf{K}_n = \frac{2}{(2\pi)^3} \sum_i \int d^3\mathbf{k} \tau_i(\mathbf{k}) \mathbf{v}_i(\mathbf{k}) \otimes \mathbf{v}_i(\mathbf{k}) \times [\varepsilon_i(\mathbf{k}) - \mu]^n \left[-\frac{\partial f(\mu, T, \varepsilon_i)}{\partial \varepsilon_i} \right], \quad (1)$$

$$\sigma = e^2 \mathbf{K}_0, \quad (2)$$

$$S = \frac{1}{eT} \mathbf{K}_1 \mathbf{K}_0^{-1}, \quad (3)$$

$$\kappa_e = \frac{1}{T} (\mathbf{K}_2 - \mathbf{K}_1^2 \mathbf{K}_0^{-1}), \quad (4)$$

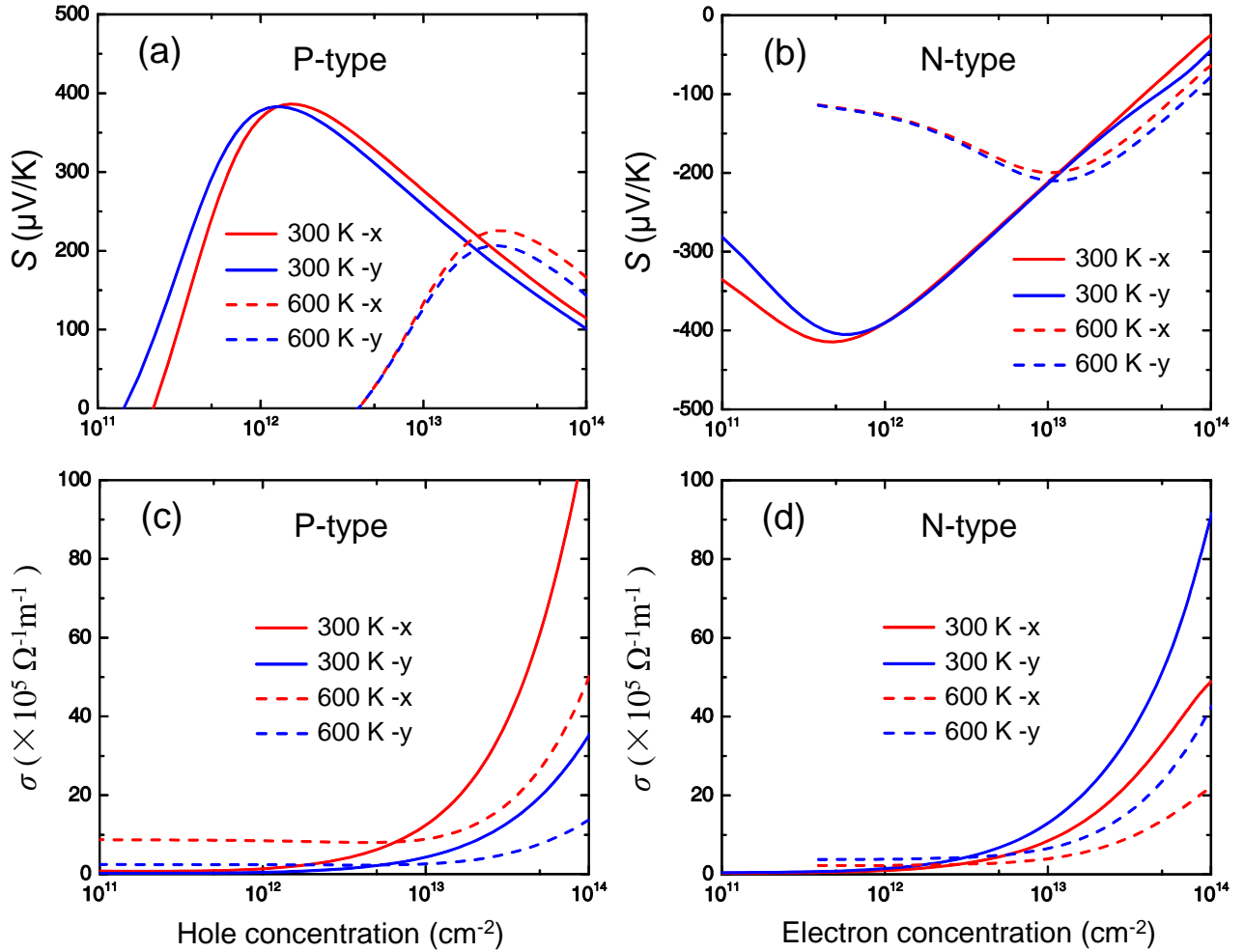


Figure 2: Calculated temperature-dependent electronic transport coefficients. (a,b) Seebeck coefficient S and (c,d) electrical conductivity σ as a function of temperature and carrier concentration (holes and electrons) for x- and y-axis at 300 K and 600 K.

in which 2 is for the spin degeneracy, $\mathbf{v}_i(\mathbf{k})$ is the electron group velocity of the wave vector \mathbf{k} and band index i . ε_i , μ , and $\tau_i(\mathbf{k})$ are electronic energy, chemical potential, and electronic relaxation time. V is the volume. Alternatively, κ_e can also be calculated through the Wiedemann-Franz law^{30,42}

$$k_e = L\sigma T, \quad (5)$$

where L is a constant called Lorenz number with a value of $2.4 \times 10^{-8} \text{ W } \Omega \text{ K}^{-2}$. The calculated k_e from Eq. (4) and Eq. (5) are the same for semiconductors, which has been verified by many previous works.^{43–45}

Here we consider two temperatures (300 K and 600 K) in the following calculations. The calculated S and σ are shown in Figure 2. For

both p-type and n-type doping, S firstly increases (absolute value) at low carrier concentration ($n < 10^{12} \text{ cm}^{-2}$), and then linearly decreases at high carrier concentration ($10^{12} \text{ cm}^{-2} < n < 10^{14} \text{ cm}^{-2}$). According to the Mahan-Sofo theory, S for degenerate 2D semiconductors can be written as⁸

$$S_{2D} = \frac{2\pi^3 k_B^2 T}{3eh^2 n} m_d^*, \quad (6)$$

where h , n , and m_d^* are the Planck constant, carrier concentration and DOS effective mass around E_F . Since electrons of 2D materials only have freedom in the plane, S_{2D} is quite different from $S_{3D} = \frac{8\pi^2 k_B^2 T}{3qh^2} \left(\frac{\pi}{3n}\right)^{(2/3)} m_d^*$ in bulk materials.⁴² Hence, there is a competition relation between n and m_d^* . For high concentration, our calculated S_{2D} of penta-silicene is inversely pro-

portional to n , which is in a good agreement with the Mahan-Sofa theory. For low concentration, S_{2D} of penta-silicene is induced by the bipolar effect in narrow band gap semiconductors.^{42,46} Interestingly, S_{2D} of penta-silicene at 300 K is generally larger than that of in 600 K. The largest S_{2D} of penta-silicene has a value of $400 \mu\text{V/K}$ at 10^{12} cm^{-2} carrier concentration for both p- and n-types, which is double of $200 \mu\text{V/K}$ of 2D SnSe⁴⁷ at the same condition.

Since the output electrical conductivity σ from the conventional Boltzmann transport theory is closely dependent on relaxation time τ , a method to evaluate τ should be applied appropriately. Considering τ in many materials generally have an order of $10 \sim 12$ ps, some works use a constant number to avoid this dilemma.^{48,49} As a matter of fact, there are many factors to impact τ , such as acoustic phonons, nonpolar optical phonons, and ionized impurities. τ in different situations has different expressions.⁵⁰ As an accepted rule of thumb, acoustic phonons play the most important role in τ and the acoustic phonon limited carrier mobility μ using deformation potential (DP) theory of 2D materials can be written as⁴²

$$\mu_{2D} = \frac{e\hbar^3 C_{2D}}{k_B T m^* m_d^* E_i^2}, \quad (7)$$

in which the parameter can be easily found elsewhere.^{42,51} The final relaxation time has a relation with mobility: $\tau = \frac{m^* \mu}{e}$. The calculated data is shown in Table 2. Note that here we use single parabolic band model from the original DP theory, which works very well for non-degenerated electronic band structure. Since penta-silicene has a distortion compared with penta-graphene, the effective mass m^* , and deformation potential constant E show a clear anisotropic behavior. Note that in the calculation of E_x and E_y , the energy of hole (electron) must be shifted with respect to the vacuum energy with an expression of $E^{h,e} - E_{vac} \propto E^{h,e} \cdot (\Delta \ell / \ell_0)$. The calculated τ of x- and y-axis, shown in Table 3, are 0.240 and 0.453 ps for electrons, while τ is 0.964 and 0.302 ps for holes, indicating a large anisotropic transport behavior.

According to the Eq. (7), σ is inversely pro-

portional to the effective mass, contrary to the situation of previous S_{2D} . The calculated σ of penta-silicene is shown in Figure 2c,d. Overall, σ significantly increases as a function of n . σ of 300 K and 600 K are comparable when $n < 10^{13} \text{ cm}^{-2}$. However, σ of 300 K increases faster than σ of 600 K when $n > 10^{13} \text{ cm}^{-2}$.

According to Eq. (5), the electronic thermal conductivity κ_e can be obtained based on σ , shown in Figure 3a,b. In semiconductors, phonons, especially acoustic phonons, are the main carrier of heat transport. Hence, at low concentration ($n < 10^{12} \text{ cm}^{-2}$), κ_e has a value of around 0.2 W/mK . As n increases, penta-silicene is increasingly doped due to the augment of corresponding σ . For a larger n , κ_e can not be neglected since more holes (electrons) are doped and the penta-silicene is more like a good conductor.^{19,30}

Generally, S decreases and σ increases as a function of carrier concentration. An admirable thermoelectric material needs large S and σ simultaneously. Power factor PF ($S^2\sigma$) is a good indicator to describe this joint effect of S and σ . The calculated PF is shown in Figure 3c,d. It increases at low concentration due to the enhancement of S and σ . Then PF decreases after climbing to the top since S is suppressed at elevated doping. For p-type, PF along the x-axis is larger than that of the y-axis. However, n-type is the opposite situation ($PF_y > PF_x$). At 300 K, the maximum PF for p-type doping is 156.40 mW/mK^2 and 40.23 mW/mK^2 at $5.09 \times 10^{13} \text{ cm}^{-2}$ concentration along the x- and y-axis, respectively. Similarly, maximum PF for n-type doping is 61.75 mW/mK^2 and 39.22 mW/mK^2 at $1.55 \times 10^{13} \text{ cm}^{-2}$ concentration along both axis at the same temperature. Such PF values are quite larger than 2D tellurium (57.3 mW/mK^2)⁴² and 2D SnSe (57.3 mW/mK^2).⁴⁷

A good thermoelectric material should satisfy that the distribution of electronic energy carriers at Fermi level is as narrow as possible, as well as high carrier velocity according to the Mahan's guideline.⁵² Subsequently, researchers find an effective approach to enhance Seebeck S and electrical conductivity σ simultaneously, where the electronic bands around E_F contain

Table 2: The calculated effective masses m_x^*/m_0 and m_y^*/m_0 , deformation potential constants E_x and E_y , 2D elastic modulus C_x^{2D} and C_y^{2D} , and carrier mobilities μ_x^{2D} and μ_y^{2D} based on Eq. (7) for x- and y-axis at 300 K.

Carrier type	m_x^*/m_0	m_y^*/m_0	E_x	E_y	C_x^{2D}	C_y^{2D}	μ_x^{2D}	μ_y^{2D}
	(G-X)	(G-Y)	(eV)	(eV)	(J m ⁻²)	(J m ⁻²)	m ² V ⁻¹ s ⁻¹	m ² V ⁻¹ s ⁻¹
electron	0.254	0.430	3.802	2.745	94.753	92.851	0.166	0.185
hole	0.224	1.106	1.546	2.737	94.753	92.851	0.756	0.048

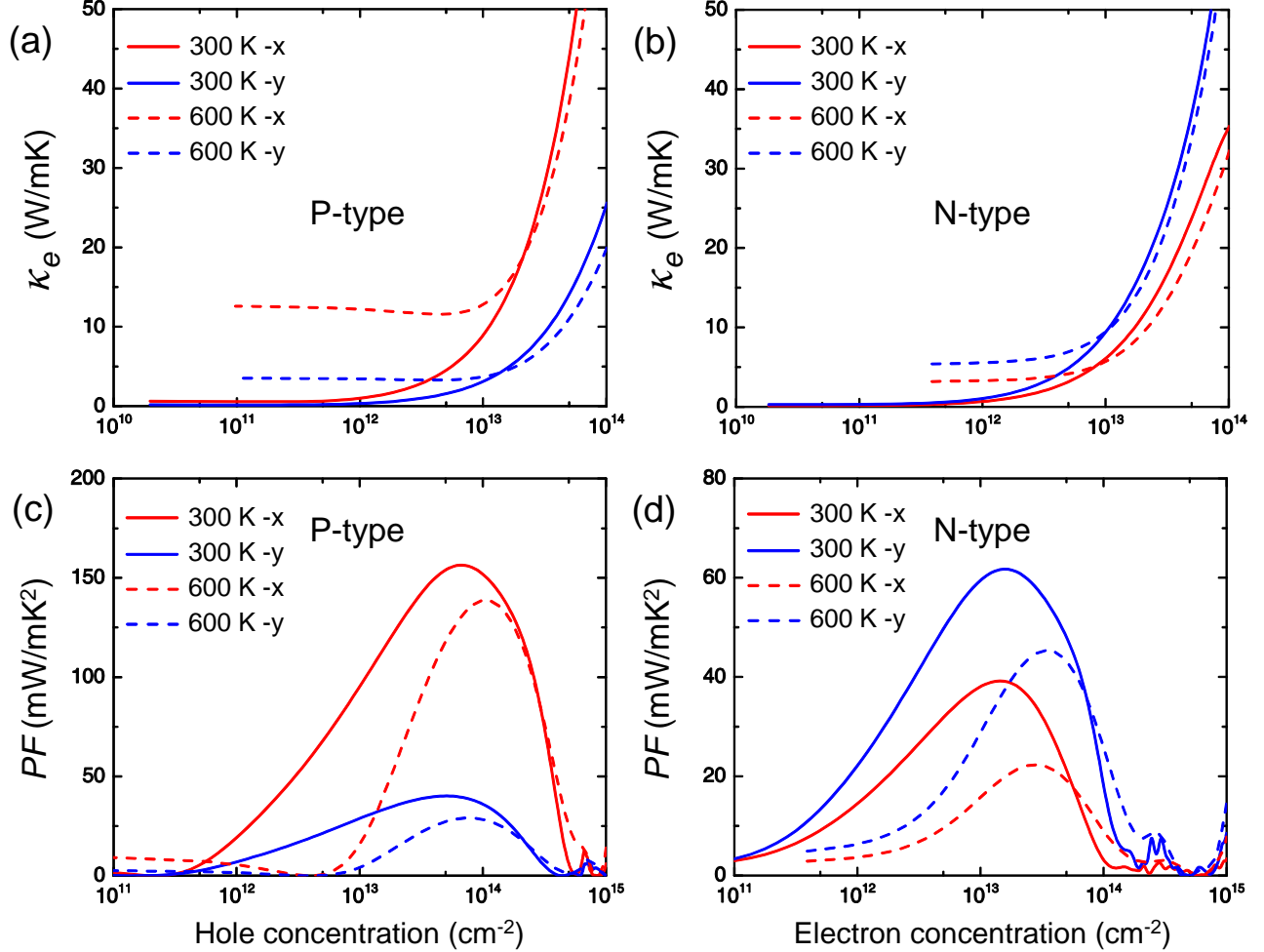


Figure 3: Calculated temperature-dependent electronic transport coefficients of penta-silicene. (a,b) electronic thermal conductivity (κ_e) and (c,d) power factor $S^2\sigma$ (PF) as a function of temperature and carrier concentration (holes and electrons) along x- and y-axis at 300 K and 600 K.

both flat and dispersive bands in the dependent momentum space. It is known as a “pudding-mold” band structure.^{53,54} Flat bands increase the DOS and dispersive bands induce high carrier velocities. It has been used to explain many prominent thermoelectric performances, such as Na_xCoO₂,⁵³ SnSe,⁵⁵ PbTe_{1-x}Se_x,¹² and

tellurium.⁴² The ultrahigh PF of penta-silicene is derived from four hole pockets and relatively flat bands with the same spirit of “pudding-mold” shown in Figure 2c,d.

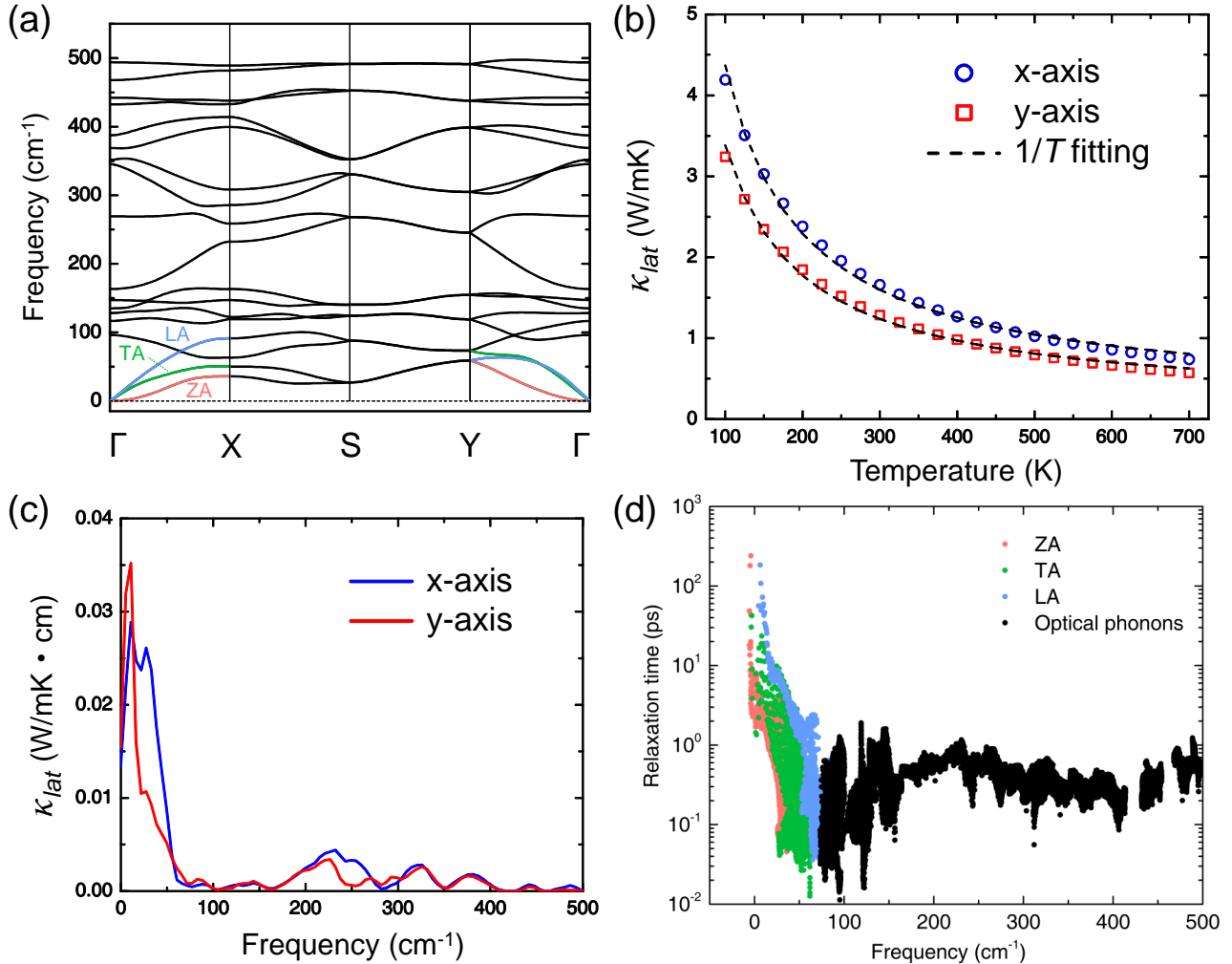


Figure 4: Lattice heat transport properties of penta-silicene. (a) phonon dispersion, (b) lattice thermal conductivity (κ_L) as a function of temperature, (c) frequency-resolved κ_L along x- and y-axis at 300 K, and (d) three-phonon relaxation time at room temperature with phonon modes resolution. The acoustic phonon branches (ZA, TA, and LA) are indicated in different colors.

Lattice thermal conductivity

Maybe the lattice thermal conductivity κ_L is the only parameter that can be tuned independently. The calculated phonon transport property of penta-silicene is shown in Figure 4. The phonon dispersion in Figure 4a is free from imaginary number, indicating a strong dynamical stability of penta-silicene. The sound velocity is defined as $v = \frac{\partial \omega}{\partial q} |_{q=0}$. The calculated v of acoustic phonon modes TA and LA are shown in Table 3 (ZA mode is a quadratic function of wave vector). More details about this parabolic ZA mode can be found in the Supporting Information. v_{TA} is 3.99 km/s and 4.70 km/s along the x- and y-axis. v_{LA} is larger than v_{TA} , having values of 4.77 km/s and 5.54 km/s along

with both directions. κ_L as a function of temperature is shown in Figure 4b. At room temperature, κ_L penta-silicene is 1.66 W/mK and 1.29 W/mK along x- and y-axis. There are two types of scatterings of phonon transport. One is the Normal process and the other one is the Umklapp (U) process. The latter is the only contributor to the final thermal resistance. The touchstone to explore the role of the U process is to study κ_L as a function of temperature. If $\kappa_L \propto \frac{1}{T}$, the U process dominates the heat transport in this material. Figure 4b of penta-silicene shows a good example of this type in heat transport behavior.

According to the Slack model, a small Θ_D generally means a small κ_L since acoustic

Table 3: The calculated electronic relaxation times τ_e and τ_h , sound velocities v_{TA} and v_{LA} , Debye temperatures Θ_{TA} and Θ_{LA} with definition of $\Theta_D = h\omega/k_B$ associated with the maximum acoustic phonon frequency, and maximum figure of merits ZT_e and ZT_h along x- and y-axis at 300 K. The subscripts “e” and “h” indicate electron and hole, respectively.

Direction	τ_e	τ_h	v_{TA}	v_{LA}	Θ_{TA}	Θ_{LA}	ZT_e	ZT_h
	(ps)	(ps)	(km/s)	(km/s)	(K)	(K)	@300 K	@300 K
G-X	0.240	0.964	3.99	4.77	72.32	131.51	2.18	3.43
G-Y	0.453	0.302	4.70	5.54	91.57	105.78	3.04	2.24

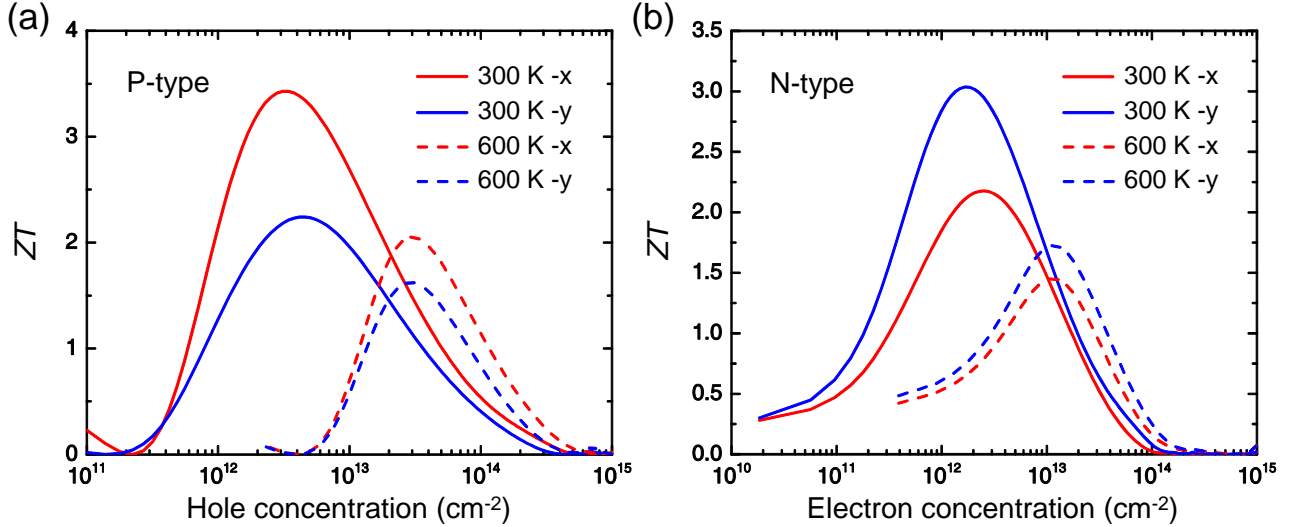


Figure 5: Calculated figure of merit ZT of (a) p-type and (b) n-type penta-silicene as a function of the carrier concentration along x- and y-axis at 300 K and 600 K.

phonons are the main carrier in heat transport. The definition is $\Theta_D = h\omega_{max}/k_B$ in which ω_{max} is the maximum frequency of the acoustic phonon branches. The calculated Θ_D of penta-silicene is shown in Table 3. The largest Θ_{LA} has a value of 131.51 K along the x-axis. This value is about one-fifth of penta-graphene ($\Theta_{LA} = 692$ K).⁵⁶ What’s more, the frequency-resolved κ_L of penta-silicene further confirms this discussion. Phonon vibrations below 50 cm^{-1} contribute most to the final κ_L and heat transport whether it is the x-axis or the y-axis. Phonon relaxation time in Figure 4d also verifies this fact. In the three branches of acoustic phonons, The LA branch has the largest phonon relaxation time compared with the ZA and TA modes. The ultralow κ_L of penta-silicene originates from the weak phonon harmonic interaction and strong anharmonic scat-

tering.^{19,57,58} We hope this low κ_L would induce a high figure of merit ZT of penta-silicene.

Figure of merit ZT

Based on the above results of electronic and phonon transport properties, one can evaluate the figure of merit ZT written as

$$ZT = \frac{S^2\sigma}{\kappa_e + \kappa_L}T. \quad (8)$$

The calculated ZT of penta-silicene for both p-type and n-type is shown in Figure 5. Interestingly, due to the high PF and low κ_L , penta-silicene shows a large ZT (> 2) at room temperature for both x- and y-axis. Specifically, maximum ZT_h (for the hole) has values of 3.43 and 2.24 at $3.42 \times 10^{12}\text{ cm}^{-2}$ and 4.60

$\times 10^{12} \text{ cm}^{-2}$ concentrations along x- and y-axis at room temperature. Similarly, maximum ZT_e (for the electron) has values of 2.18 and 3.04 at $2.51 \times 10^{12} \text{ cm}^{-2}$ and $1.85 \times 10^{12} \text{ cm}^{-2}$ along x- and y-axis at 300 K. In a graphene-based field-effect transistor, a doping level up to $4 \times 10^{14} \text{ cm}^{-2}$ for both electrons and holes has been reached by electrical gating⁵⁹ and ionic liquid injection.⁶⁰ Due to the portability of the experimental technique, 2D material, like graphene, MoS₂, and black phosphorus, generally can reach $4 \times 10^{14} \text{ cm}^{-2}$ for both electrons and holes doping level. Note that our carrier concentrations ($< 4 \times 10^{14} \text{ cm}^{-2}$) all are reachable in these current experimental technique. Therefore, our result indicates that monolayer penta-silicene is a promising thermoelectric material.

Conclusion and Discussion

According to Eq. (8), the figure of merit ZT is closely related to the temperature. Generally, ZT increases when temperature increases, such as SnSe with ZT of 2.6 ± 0.3 at 923 K⁵⁵ and PbTePbS pseudo-binary with ZT of 2.3 at 923 K.⁶¹ Taking into account the application of daily life, near room temperature thermoelectric materials with high ZT are desirable. There is no doubt that Bi₂Te₃-based thermoelectric materials still dominate around room temperature. However, the tellurium element has very low reserves on earth and much expensive. How to find inexpensive thermoelectric material that works efficiently at room temperature is still an open question. Very recently, some researchers have made progress in this direction. For example, Mg₃Bi₂ alloy has a ZT of 0.9 at 350 K.⁶² Penta-silicene with ZT of 3.43 probably enriches the room temperature thermoelectric materials. Besides, how to manipulate defects, lattice symmetry, spin, and electron-phonon coupling to further enhance room temperature ZT is one of the cutting edges in the thermoelectric field.

For 2D materials, stability is the most important before the property. As a matter of fact, metastable phases are quite common in con-

densed matter. Materials science overwhelmingly deals with metastable states. Besides penta-silicene, many simple light-element compounds including most hydrocarbons, nitrogen oxides, hydrides, carbides, carbon monoxide (CO), alcohols and glycerin are also metastable at ambient condition. Nevertheless, the ubiquitous metastable phases do not produce a bad effect on their vast and tremendous applications in modern industrial societies and our daily life. The world has been varied and diverse due to the fact that the metastable states provide the complexity of structures and energy transformation. Furthermore, previous works have successfully obtained penta-silicene nanoribbon on Ag(110) with exotic electronic properties.^{4-6,21} At the energy level, the cohesive energy E_c of penta-silicene is 3.92 eV/atom that is comparable with the 3.71 eV/atom^{32,33} of silicene (hexagonal symmetry with 2 atoms in the primitive cell) and 3.61 eV/atom^{34,35} of black phosphorene. Note that above two metastable 2D materials, at present, can be easily obtained in experiment based on the advanced experimental technique such as creating a complex chemical environment and variable substrate effect. Besides, we also calculate other two allotropes of penta-silicene. There are Si-*Cmma* and Si-*Pmma*.³⁸ The calculated E_c of Si-*Cmma* and Si-*Pmma* are 4.17 eV/atom and 4.18 eV/atom, relatively more stable than penta-silicene.

Moreover, we offer three very promising experimental approaches to make free standing penta-silicene potentially. Besides, these methods also have great potential for other 2D materials. “Geometrical frustration” was first raised by Joel Therrien who are synthesizing the penta-graphene and other free-standing carbon rings, such as the U-carbon.⁶³ As far as we can see, penta-silicene has no counterpart in the corresponding bulk material. This fact is quite different from graphene and graphite. Crystalline oxide perovskites, like penta-silicene, also cannot be obtained by mechanical exfoliation. However, monolayer freestanding crystalline oxide perovskites has been grown by “reactive molecular beam epitaxy”.⁶⁴ Besides, free-standing monolayer amorphous carbon has successfully been created by “laser-

assisted chemical vapor deposition” method.⁶⁵ This monolayer amorphous carbon contains 5-, 6-, 7-, and 8-membered carbon rings. Note that penta-silicene only consists of 5-membered silicon rings. Encouraged by these above advanced technologies in the experimental cutting edge, we conclude monolayer free-standing penta-silicene and other novel nanostructures can also be obtained on the near horizon.

Sometimes, the figure of merit ZT based on the mobility μ in Eq. (7) is a little overestimated since acoustic phonon is not the only factor to impact the μ that determines the final ZT . As we mentioned before, nonpolar optical phonons, and ionized impurities also influence μ . Generally, the impact of these two factors can be neglected and the role of longitudinal acoustic phonons is dominant.^{12,51,66,67} Given that realistic calculation of couplings between nonpolar optical phonons and electrons, ionized impurities and electrons are beyond our current computing capabilities, they are interesting open questions that deserve further exploration.

DP theory is based on the rigid band approximation. Surprisingly, this approximation works well for most cases when the electronic bands around the fermi level are not highly degenerate.^{42,68} Besides, VASP, Quantum ESPRESSO, and BoltzTraP softwares,²⁷⁻³⁰ to name a few, also can add electrons into or remove electrons from the system through a compensating uniform charge background of opposite sign to maintain charge neutrality, which verifies the correctness of this approximation additionally.

DP theory has been widely used and has been successful in calculating the intrinsic (free-standing and defects-free) mobility, which can be found everywhere. Certainly, almost any theoretical model has assumptions, either large or small, such as famous density functional theory, Dulong-Petit law (high temperature) and even Newton’s laws of motion (inertial system). DP theory is also included. As a matter of fact, in the DP theory, only the longitudinal-acoustic phonon is considered without any dispersion and the electron-phonon matrix is expressed by the DP constant and the elastic constant that are described in the Eq. (7). The optical phonon scatterings are absent in the DP

theory. However, DP theory’s results are qualitatively and even quantitatively reasonable in many cases compared with the full evaluation of electron-phonon coupling.⁶⁹ Since this calculation is far beyond our current computational capabilities, hence, we suggest leaving the e-ph coupling as an open question, which should be explored further.

How a 2D functional material, like our penta-silicene, is to be used in bulk devices? There are 4 options to integrate bulk materials with 2D materials for physical coupling and applications.⁷⁰ On the one hand, one can construct 2D materials on 3D materials (2D-on-3D) heterostructures. The technique methods are Van der Waals epitaxy (vdWE), wet transfer and metal-induced quasi-dry transfer process. On the other hand, the realization of 3D-to-2D heterostructures is still at a premature stage. But the relevant experiment is growing fast, which has significantly broadened the material beyond conventional 3D materials-based heterostructures.

In summary, we have calculated the thermoelectric performance of monolayer penta-silicene by first principles. It has good thermal, dynamical, and mechanical stability compared with many other typical 2D materials, such as hexagonal silicene and black phosphorous. Lattice thermal conductivities of penta-silicene have values of 1.66 and 1.29 W/mK along x- and y-axis, respectively. Superior electronic properties originate from the “pudding-mold-like” shape of valence bands around the Fermi level. Ultralow thermal conductivity and high power factor collaboratively lead to an ultrahigh ZT of penta-silicene. At room temperature, maximum ZT has values of 3.43 and 3.04 for hole doping and electron doping, respectively. Our work has indicated that penta-silicene is a promising thermoelectric material, especially near room temperature. Layer-dependent thermoelectric property of penta-silicene deserves more follow up study in the future.

Author Information

Corresponding Author

ORCID

Zhibin Gao: 0000-0002-6843-381X

Supporting Information

The Supporting Information is available free of charge on the ACS Publications website via the Internet at <https://pubs.acs.org/journal/aamick>.

Room temperature lattice thermal conductivity of penta-silicene as a function of the cutoff for the interaction range of anharmonic force constants and phonon dispersion superposed on the spectra from continuum theory.

Notes

The authors declare no competing financial interest.

Acknowledgement

We are grateful to Wu Li for the kind guidance on calculation of lattice thermal conductivity. We acknowledge Jinyang Xi for many fruitful discussions and good suggestions. We also thank Wen Shi and Tianqi Deng for valuable discussions and kind help. We acknowledge the financial support from MOE tier 1 funding of NUS Faculty of Science, Singapore (Grant No. R-144-000-402-114).

References

- (1) Goodilin, E. A.; Weiss, P. S.; Gogotsi, Y. Nanotechnology Facets of the Periodic Table of Elements. *ACS Nano* **2019**, *13*, 10879–10886.
- (2) Tao, L.; Cinquanta, E.; Chiappe, D.; Grazianetti, C.; Fanciulli, M.; Dubey, M.; Molle, A.; Akinwande, D. Silicene Field-Effect Transistors Operating at Room Temperature. *Nat. Nanotechnol.* **2015**, *10*, 227.
- (3) Tsai, W.-F.; Huang, C.-Y.; Chang, T.-R.; Lin, H.; Jeng, H.-T.; Bansil, A. Gated Silicene as a Tunable Source of Nearly 100% Spin-Polarized Electrons. *Nat. Commun.* **2013**, *4*, 1500.
- (4) Cerdá, J. I.; Sławińska, J.; Le Lay, G.; Marele, A. C.; Gómez-Rodríguez, J. M.; Dávila, M. E. Unveiling the Pentagonal Nature of Perfectly Aligned Single- and Double-Strand Si Nano-Ribbons on Ag(110). *Nat. Commun.* **2016**, *7*, 13076.
- (5) Prévot, G.; Hogan, C.; Leoni, T.; Bernard, R.; Moyen, E.; Masson, L. Si Nanoribbons on Ag(110) Studied by Grazing-Incidence X-Ray Diffraction, Scanning Tunneling Microscopy, and Density-Functional Theory: Evidence of a Pentamer Chain Structure. *Phys. Rev. Lett.* **2016**, *117*, 276102.
- (6) Sheng, S.; Ma, R.; Wu, J.-b.; Li, W.; Kong, L.; Cong, X.; Cao, D.; Hu, W.; Gou, J.; Luo, J.-W.; Cheng, P.; Tan, P.-H.; Jiang, Y.; Chen, L.; Wu, K. The Pentagonal Nature of Self-Assembled Silicon Chains and Magic Clusters on Ag (110). *Nano Lett.* **2018**, *18*, 2937–2942.
- (7) He, J.; Tritt, T. M. Advances in Thermoelectric Materials Research: Looking Back and Moving Forward. *Science* **2017**, *357*, eaak9997.
- (8) Snyder, G.; Toberer, E. Complex Thermoelectric Materials. *Nat. Mater.* **2008**, *7*, 105–114.
- (9) Lee, S.; Esfarjani, K.; Luo, T.; Zhou, J.; Tian, Z.; Chen, G. Resonant Bonding Leads to Low Lattice Thermal Conductivity. *Nat. Commun.* **2014**, *5*, 3525.
- (10) Nielsen, M. D.; Ozolins, V.; Heremans, J. P. Lone Pair Electrons Minimize Lattice Thermal Conductivity. *Energy Environ. Sci.* **2013**, *6*, 570–578.
- (11) Heremans, J. P.; Jovovic, V.; Toberer, E. S.; Saramat, A.; Kurosaki, K.; Charoenphakdee, A.; Yamanaka, S.; Snyder, G. J. Enhancement of Thermoelectric Efficiency in PbTe by Distortion of the Electronic Density of States. *Science* **2008**, *321*, 554–557.

- (12) Pei, Y.; Shi, X.; LaLonde, A.; Wang, H.; Chen, L.; Snyder, G. J. Convergence of Electronic Bands for High Performance Bulk Thermoelectrics. *Nature* **2011**, *473*, 66.
- (13) Liu, W.; Tan, X.; Yin, K.; Liu, H.; Tang, X.; Shi, J.; Zhang, Q.; Uher, C. Convergence of Conduction Bands as a Means of Enhancing Thermoelectric Performance of n -Type $\text{Mg}_2\text{Si}_{1-x}\text{Sn}_x$ Solid Solutions. *Phys. Rev. Lett.* **2012**, *108*, 166601.
- (14) Dresselhaus, M. S.; Chen, G.; Tang, M. Y.; Yang, R.; Lee, H.; Wang, D.; Ren, Z.; Fleurial, J.-P.; Gogna, P. New Directions for Low-Dimensional Thermoelectric Materials. *Adv. Mater.* **2007**, *19*, 1043–1053.
- (15) Zhang, S.; Zhou, J.; Wang, Q.; Chen, X.; Kawazoe, Y.; Jena, P. Penta-Graphene: A New Carbon Allotrope. *Proc. Natl. Acad. Sci. U. S. A.* **2015**, *112*, 2372–2377.
- (16) Ressouche, E.; Simonet, V.; Canals, B.; Gospodinov, M.; Skumryev, V. Magnetic Frustration in an Iron-Based Cairo Pentagonal Lattice. *Phys. Rev. Lett.* **2009**, *103*, 267204.
- (17) Wu, X.; Varshney, V.; Lee, J.; Zhang, T.; Wohlwend, J. L.; Roy, A. K.; Luo, T. Hydrogenation of Penta-Graphene Leads to Unexpected Large Improvement in Thermal Conductivity. *Nano Lett.* **2016**, *16*, 3925–3935.
- (18) Liu, H.; Qin, G.; Lin, Y.; Hu, M. Disparate Strain Dependent Thermal Conductivity of Two-Dimensional Penta-Structures. *Nano Lett.* **2016**, *16*, 3831–3842.
- (19) Gao, Z.; Zhang, Z.; Liu, G.; Wang, J.-S. Ultralow Lattice Thermal Conductivity of Monolayer Penta-Silicene and Penta-Germanene. *Phys. Chem. Chem. Phys.* **2019**, 26033–26040.
- (20) Oyedele, A. D.; Yang, S.; Feng, T.; Haglund, A. V.; Gu, Y.; Puretzky, A. A.; Briggs, D.; Rouleau, C. M.; Chisholm, M. F.; Unocic, R. R.; Mandrus, D.; Meyer, H. M.; Pantelides, S. T.; Geohagan, D. B.; Xiao, K. Defect-Mediated Phase Transformation in Anisotropic 2D PdSe_2 Crystals for Seamless Electrical Contacts. *J. Am. Chem. Soc.* **2019**, *141*, 8928–8936.
- (21) Guo, Y.; Zhang, C.; Zhou, J.; Wang, Q.; Jena, P. Lattice Dynamic and Instability in Pentasilicene: A Light Single-Element Ferroelectric Material With High Curie Temperature. *Phys. Rev. Applied* **2019**, *11*, 064063.
- (22) Blöchl, P. E. Projector Augmented-Wave Method. *Phys. Rev. B: Condens. Matter Mater. Phys.* **1994**, *50*, 17953–17979.
- (23) Kresse, G.; Joubert, D. From Ultra-soft Pseudopotentials to the Projector Augmented-Wave Method. *Phys. Rev. B: Condens. Matter Mater. Phys.* **1999**, *59*, 1758–1775.
- (24) Perdew, J. P.; Burke, K.; Ernzerhof, M. Generalized Gradient Approximation Made Simple. *Phys. Rev. Lett.* **1996**, *77*, 3865–3868.
- (25) Heyd, J.; Scuseria, G. E.; Ernzerhof, M. Hybrid Functionals Based on a Screened Coulomb Potential. *J. Chem. Phys.* **2003**, *118*, 8207–8215.
- (26) Krukau, A. V.; Vydrov, O. A.; Izmaylov, A. F.; Scuseria, G. E. Influence of the Exchange Screening Parameter on the Performance of Screened Hybrid Functionals. *J. Chem. Phys.* **2006**, *125*, 224106.
- (27) Kresse, G.; Furthmüller, J. Efficient Iterative Schemes for *Ab Initio* Total-Energy Calculations Using A Plane-Wave Basis Set. *Phys. Rev. B: Condens. Matter Mater. Phys.* **1996**, *54*, 11169–11186.
- (28) Kresse, G.; Furthmüller, J. Efficiency of *Ab-Initio* Total Energy Calculations for Metals and Semiconductors Using A

- Plane-Wave Basis Set. *Comput. Mater. Sci.* **1996**, *6*, 15–50.
- (29) Kresse, G.; Hafner, J. *Ab Initio* Molecular-Dynamics Simulation of the Liquid-Metal–Amorphous-Semiconductor Transition in Germanium. *Phys. Rev. B: Condens. Matter Mater. Phys.* **1994**, *49*, 14251–14269.
- (30) Madsen, G. K.; Singh, D. J. BoltzTraP. A Code for Calculating Band-Structure Dependent Quantities. *Comput. Phys. Commun.* **2006**, *175*, 67–71.
- (31) Li, W.; Carrete, J.; Katcho, N. A.; Mingo, N. ShengBTE: A Solver of the Boltzmann Transport Equation for Phonons. *Comput. Phys. Commun.* **2014**, *185*, 1747.
- (32) Fleurence, A.; Friedlein, R.; Ozaki, T.; Kawai, H.; Wang, Y.; Yamada-Takamura, Y. Experimental Evidence for Epitaxial Silicene on Diboride Thin Films. *Phys. Rev. Lett.* **2012**, *108*, 245501.
- (33) Feng, B.; Ding, Z.; Meng, S.; Yao, Y.; He, X.; Cheng, P.; Chen, L.; Wu, K. Evidence of Silicene in Honeycomb Structures of Silicon on Ag (111). *Nano Lett.* **2012**, *12*, 3507–3511.
- (34) Liu, H.; Neal, A. T.; Zhu, Z.; Luo, Z.; Xu, X.; Tománek, D.; Ye, P. D. Phosphorene: An Unexplored 2D Semiconductor with A High Hole Mobility. *ACS Nano* **2014**, *8*, 4033–4041.
- (35) Li, L.; Yu, Y.; Ye, G. J.; Ge, Q.; Ou, X.; Wu, H.; Feng, D.; Chen, X. H.; Zhang, Y. Black Phosphorus Field-Effect Transistors. *Nat. Nanotechnol.* **2014**, *9*, 372.
- (36) Liu, D.; Every, A. G.; Tománek, D. Continuum Approach for Long-Wavelength Acoustic Phonons in Quasi-Two-Dimensional Structures. *Phys. Rev. B: Condens. Matter Mater. Phys.* **2016**, *94*, 165432.
- (37) Gao, Z.; Dong, X.; Li, N.; Ren, J. Novel Two-Dimensional Silicon Dioxide with In-Plane Negative Poissons Ratio. *Nano Lett.* **2017**, *17*, 772–777.
- (38) Zhou, N.; Zhou, P.; Li, J.; He, C.; Zhong, J. Si-Cmma: A Silicon Thin Film with Excellent Stability and Dirac Nodal Loop. *Phys. Rev. B: Condens. Matter Mater. Phys.* **2019**, *100*, 115425.
- (39) Gao, Z.; Liu, D.; Tománek, D. Two-Dimensional Mechanical Metamaterials with Unusual Poisson Ratio Behavior. *Phys. Rev. Applied* **2018**, *10*, 064039.
- (40) Zhu, Z.; Cai, X.; Yi, S.; Chen, J.; Dai, Y.; Niu, C.; Guo, Z.; Xie, M.; Liu, F.; Cho, J.-H.; Jia, Y.; Zhang, Z. Multivalency-Driven Formation of Te-Based Monolayer Materials: A Combined First-Principles and Experimental study. *Phys. Rev. Lett.* **2017**, *119*, 106101.
- (41) Guo, R.; Wang, X.; Kuang, Y.; Huang, B. First-Principles Study of Anisotropic Thermoelectric Transport Properties of IV-VI Semiconductor Compounds SnSe and SnS. *Phys. Rev. B: Condens. Matter Mater. Phys.* **2015**, *92*, 115202.
- (42) Gao, Z.; Liu, G.; Ren, J. High Thermoelectric Performance in Two-Dimensional Tellurium: An *Ab Initio* Study. *ACS Appl. Mater. Interfaces* **2018**, *10*, 40702–40709.
- (43) Li, M.; Wang, N.; Jiang, M.; Xiao, H.; Zhang, H.; Liu, Z.; Zu, X.; Qiao, L. Improved Thermoelectric Performance of Bilayer Bi₂O₂Se by the Band Convergence Approach. *J. Mater. Chem. C* **2019**, *7*, 11029–11039.
- (44) Toberer, E. S.; Baranowski, L. L.; Dames, C. Advances in Thermal Conductivity. *Annu. Rev. Mater. Res.* **2012**, *42*, 179–209.
- (45) Wang, F. Q.; Guo, Y.; Wang, Q.; Kawazoe, Y.; Jena, P. Exceptional Thermoelectric Properties of Layered GeAs₂. *Chem. Mater.* **2017**, *29*, 9300–9307.

- (46) Bahk, J.-H.; Shakouri, A. Minority Carrier Blocking to Enhance the Thermoelectric Figure of Merit in Narrow-Band-Gap Semiconductors. *Phys. Rev. B: Condens. Matter Mater. Phys.* **2016**, *93*, 165209.
- (47) Chang, C.; Wu, M.; He, D.; Pei, Y.; Wu, C.-F.; Wu, X.; Yu, H.; Zhu, F.; Wang, K.; Chen, Y.; Huang, L.; Li, J.-F.; He, J.; Zhao, L.-D. 3D Charge and 2D Phonon Transports Leading to High Out-of-Plane ZT in n-Type SnSe Crystals. *Science* **2018**, *360*, 778–783.
- (48) Bilc, D. I.; Hautier, G.; Waroquiers, D.; Rignanese, G.-M.; Ghosez, P. Low-Dimensional Transport and Large Thermoelectric Power Factors in Bulk Semiconductors by Band Engineering of Highly Directional Electronic States. *Phys. Rev. Lett.* **2015**, *114*, 136601.
- (49) He, J.; Amsler, M.; Xia, Y.; Naghavi, S. S.; Hegde, V. I.; Hao, S.; Goedecker, S.; Ozoliņš, V.; Wolverton, C. Ultralow Thermal Conductivity in Full Heusler Semiconductors. *Phys. Rev. Lett.* **2016**, *117*, 046602.
- (50) Popescu, A.; Woods, L. M.; Martin, J.; Nolas, G. S. Model of Transport Properties of Thermoelectric Nanocomposite Materials. *Phys. Rev. B: Condens. Matter Mater. Phys.* **2009**, *79*, 205302.
- (51) Qiao, J.; Kong, X.; Hu, Z.-X.; Yang, F.; Ji, W. High-Mobility Transport Anisotropy and Linear Dichroism in Few-Layer Black Phosphorus. *Nat. Commun.* **2014**, *5*, 4475.
- (52) Mahan, G. D.; Sofo, J. O. The Best Thermoelectric. *Proc. Natl. Acad. Sci. U. S. A.* **1996**, *93*, 7436–7439.
- (53) Kuroki, K.; Arita, R. “Pudding Mold” Band Drives Large Thermopower in Na_xCoO_2 . *J. Phys. Soc. Jpn.* **2007**, *76*, 083707.
- (54) Usui, H.; Suzuki, K.; Kuroki, K.; Nakano, S.; Kudo, K.; Nohara, M. Large Seebeck Effect in Electron-Doped FeAs_2 Driven by a Quasi-One-Dimensional Pudding-Mold-Type Band. *Phys. Rev. B: Condens. Matter Mater. Phys.* **2013**, *88*, 075140.
- (55) Zhao, L.-D.; Lo, S.-H.; Zhang, Y.; Sun, H.; Tan, G.; Uher, C.; Wolverton, C.; Dravid, V. P.; Kanatzidis, M. G. Ultralow Thermal Conductivity and High Thermoelectric Figure of Merit in SnSe Crystals. *Nature* **2014**, *508*, 373–390.
- (56) Wang, F. Q.; Yu, J.; Wang, Q.; Kawazoe, Y.; Jena, P. Lattice Thermal Conductivity of Penta-Graphene. *Carbon* **2016**, *105*, 424–429.
- (57) Bao, H.; Chen, J.; Gu, X.; Cao, B. A Review of Simulation Methods in Micro/Nanoscale Heat Conduction. *ES Energy & Environment* **2018**, *1*, 16–55.
- (58) Ouyang, T.; Jiang, E.; Tang, C.; Li, J.; He, C.; Zhong, J. Thermal and Thermoelectric Properties of Monolayer Indium Triphosphide (InP_3): A First-Principles Study. *J. Mater. Chem. A* **2018**, *6*, 21532–21541.
- (59) Efetov, D. K.; Kim, P. Controlling Electron-Phonon Interactions in Graphene at Ultrahigh Carrier Densities. *Phys. Rev. Lett.* **2010**, *105*, 256805.
- (60) Chuang, H.-J.; Tan, X.; Ghimire, N. J.; Perera, M. M.; Chamlagain, B.; Cheng, M. M.-C.; Yan, J.; Mandrus, D.; Tománek, D.; Zhou, Z. High Mobility WSe_2 p-and n-Type Field-Effect Transistors Contacted by Highly Doped Graphene for Low-Resistance Contacts. *Nano Lett.* **2014**, *14*, 3594–3601.
- (61) Wu, D.; Zhao, L.-D.; Tong, X.; Li, W.; Wu, L.; Tan, Q.; Pei, Y.; Huang, L.; Li, J.-F.; Zhu, Y.; Kanatzidis, M. G.; He, J. Superior Thermoelectric Performance in PbTe-PbS Pseudo-Binary: Extremely Low Thermal Conductivity and Modulated Carrier Concentration. *Energy Environ. Sci.* **2015**, *8*, 2056–2068.

- (62) Mao, J.; Zhu, H.; Ding, Z.; Liu, Z.; Gamage, G. A.; Chen, G.; Ren, Z. High Thermoelectric Cooling Performance of n-Type Mg_3Bi_2 -Based Materials. *Science* **2019**, *365*, 495–498.
- (63) Gibbs, W. W. A New Form of Pure Carbon Dazzles and Attracts. *Science* **2019**, *366*, 782–783.
- (64) Ji, D.; Cai, S.; Paudel, T. R.; Sun, H.; Zhang, C.; Han, L.; Wei, Y.; Zang, Y.; Gu, M.; Zhang, Y. Freestanding Crystalline Oxide Perovskites Down To the Monolayer Limit. *Nature* **2019**, *570*, 87.
- (65) Toh, C.-T.; Zhang, H.; Lin, J.; Mayorov, A. S.; Wang, Y.-P.; Orofeo, C. M.; Ferry, D. B.; Andersen, H.; Kakenov, N.; Guo, Z.; Abidi, I. H.; Sims, H.; Suenaga, K.; Pantelides, S. T.; zylmaz, B. Synthesis and Properties of Free-Standing Monolayer Amorphous Carbon. *Nature* **2020**, *577*, 199–203.
- (66) Bardeen, J.; Shockley, W. Deformation Potentials and Mobilities in Non-Polar Crystals. *Phys. Rev.* **1950**, *80*, 72–80.
- (67) Wang, H.; Pei, Y.; LaLonde, A. D.; Snyder, G. J. Weak Electron–Phonon Coupling Contributing to High Thermoelectric Performance in N-Type PbSe. *Proc. Natl. Acad. Sci. U. S. A.* **2012**, *109*, 9705–9709.
- (68) Gao, Z.; Zhou, Z.; Tománek, D. Degenerately Doped Transition Metal Dichalcogenides as Ohmic Homojunction Contacts to Transition Metal Dichalcogenide Semiconductors. *ACS Nano* **2019**, *13*, 5103–5111.
- (69) Nakamura, Y.; Zhao, T.; Xi, J.; Shi, W.; Wang, D.; Shuai, Z. Intrinsic Charge Transport in Stanene: Roles of Bucklings and Electron–Phonon Couplings. *Adv. Electron. Mater.* **2017**, *3*, 1700143.
- (70) Bae, S.-H.; Kum, H.; Kong, W.; Kim, Y.; Choi, C.; Lee, B.; Lin, P.; Park, Y.; Kim, J. Integration of bulk materials

with two-dimensional materials for physical coupling and applications. *Nat. Mater.* **2019**, *18*, 550–560.

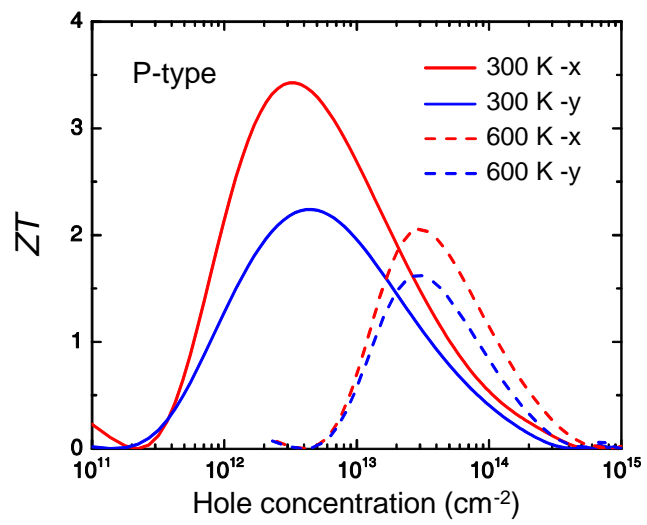
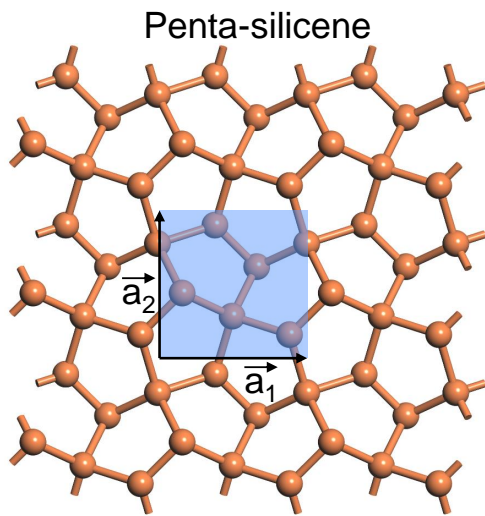


Table of Contents Graphic